Neuron
Article

Insulin Receptor Signaling Regulates Synapse Number, Dendritic Plasticity, and Circuit Function In Vivo

Shu-Ling Chiu,[1] Chih-Ming Chen,[1] and Hollis T. Cline[1,*]
[1]Watson School of Biological Sciences and Cold Spring Harbor Laboratory, Cold Spring Harbor, NY 11724, USA
*Correspondence: cline@cshl.edu
DOI 10.1016/j.neuron.2008.04.014

SUMMARY

Insulin receptor signaling has been postulated to play a role in synaptic plasticity; however, the function of the insulin receptor in CNS is not clear. To test whether insulin receptor signaling affects visual system function, we recorded light-evoked responses in optic tectal neurons in living *Xenopus* tadpoles. Tectal neurons transfected with dominant-negative insulin receptor (dnIR), which reduces insulin receptor phosphorylation, or morpholino against insulin receptor, which reduces total insulin receptor protein level, have significantly smaller light-evoked responses than controls. dnIR-expressing neurons have reduced synapse density as assessed by EM, decreased AMPA mEPSC frequency, and altered experience-dependent dendritic arbor structural plasticity, although synaptic vesicle release probability, assessed by paired-pulse responses, synapse maturation, assessed by AMPA/NMDA ratio and ultrastructural criteria, are unaffected by dnIR expression. These data indicate that insulin receptor signaling regulates circuit function and plasticity by controlling synapse density.

INTRODUCTION

The insulin receptor is a receptor tyrosine kinase well studied in its function in regulating peripheral glucose metabolism. Although expression of the insulin receptor in the brain was discovered decades ago (Havrankova et al., 1978; Unger et al., 1989), insulin receptor function in this classical ''insulin-insensitive'' organ remains largely unknown. Insulin receptors are intrinsic disulfide-linked dimers, composed of an extracellular insulin-binding domain and an intracellular tyrosine kinase. Ligand binding and subsequent kinase activity initiate a cascade of phosphorylation events that lead to different biological functions. Emerging data support the idea that the brain is an insulin target and that brain insulin receptor signaling plays diverse roles in neuronal survival (Valenciano et al., 2006), synaptic plasticity (Beattie et al., 2000; Man et al., 2000; Passafaro et al., 2001; Skeberdis et al., 2001; Wan et al., 1997), and learning and memory (Dou et al., 2005; Zhao et al., 1999). Brain insulin is released from neurons upon depolarization (Clarke et al., 1986), and the insulin receptor substrate, IRSp53, translocates to synapses in response to activity (Hori et al., 2005), suggesting that insulin receptor signaling may increase in an activity-dependent manner. Studies in cell culture suggest that insulin receptor signaling reportedly regulates spine density and neurite growth (Choi et al., 2005; Govind et al., 2001); however, the role of insulin receptor signaling in controlling structure and function of CNS circuits has not yet been demonstrated in vivo.

Here, we tested whether insulin receptor signaling is involved in synaptic connectivity, dendritic plasticity, and circuit function in the visual system of living *Xenopus laevis* tadpoles. The retinotectal circuit of *Xenopus*, in which tectal neurons receive direct visual input from the retinal ganglion cells (RGCs) in the eye (Figure 1A), is a powerful experimental system to study both structural (Haas et al., 2006; Sin et al., 2002) and functional plasticity (Aizenman and Cline, 2007; Engert et al., 2002; Zhang et al., 2000) in vivo. Functionally, the visual circuitry is relatively simple and well defined, which allows us to record visual responses to physiological light stimuli and study sensory experience-dependent mechanisms. Structurally, the tadpole is transparent, which allows us to image changes in dendritic structure of fluorescently labeled neurons over hours to days in an intact animal. We manipulated insulin receptor protein level by morpholino-mediated insulin receptor knockdown or insulin receptor signaling by expression of wild-type insulin receptor (wtIR) or dnIR in single tectal neurons and show that the insulin receptor plays a crucial role in visual circuit function by affecting tectal neuronal responses to visual stimulation. Moreover, we demonstrate that insulin receptor function affects circuit properties by regulating synapse number according to both electrophysiological and ultrastructural criteria. Furthermore, multiphoton time-lapse imaging data show that the insulin receptor mediates experience-dependent dendritic structural plasticity. Our study provides evidence that insulin receptor signaling regulates the maintenance of synapses and contributes not only to the processing of sensory information but also to experience-dependent structural plasticity that is required for the incorporation of neurons into brain circuits.

RESULTS

Insulin Receptor Localization in the CNS of *Xenopus* Tadpole

In the mammalian CNS, the insulin receptor is widely but selectively expressed in specific brain regions, such as olfactory bulb,

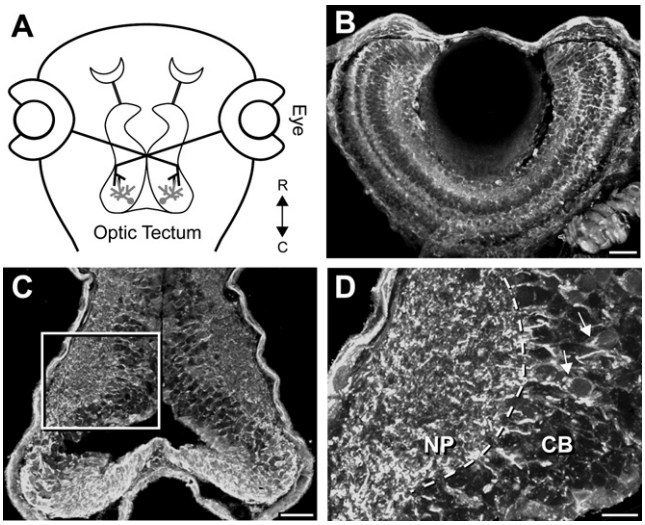

Figure 1. Insulin Receptor Localization in the Visual System of *X. laevis*

(A) Diagram of the *Xenopus* visual circuit. Optic tectal neurons receive direct visual input from retina ganglion cells of the eye.

(B–D) Insulin receptor immunostaining in the eye (B) and brain (C and D). Insulin receptor is widely distributed in the *Xenopus* visual circuit. Area in box in (C) is enlarged in (D). Insulin receptor is present in the cell body (CB) region and dendrites and is concentrated in the neuropil (NP) of the tectum and retina. R, rostral; C, caudal; arrow, primary dendrites of tectal neurons. Scale bars: 50 μm in (B) and (C), 20 μm in (D).

cerebral cortex, hypothalamus, hippocampus, and cerebellum (Havrankova et al., 1978; Unger et al., 1989). Insulin receptor immunoreactivity is widely distributed in the *Xenopus* retinotectal circuit (Figure 1). Within the optic tectum, insulin receptor immunoreactivity localizes to neurons throughout the rostro-caudal axis of neuronal maturation (Cline et al., 1996), suggesting that the insulin receptor functions throughout a neuron's lifetime. Insulin receptor immunoreactivity is absent from the nucleus. It is present in the major dendrites and exhibits an intense punctate pattern in the neuropil (Figure 1D). In the eye, insulin receptor immunoreactivity is present in all cellular layers, including the RGC layer, and exhibits a punctate pattern in the synaptic layers (Figure 1B).

Manipulation of Insulin Receptor Signaling In Vivo

To study the function of insulin receptor signaling in the CNS, we cloned *Xenopus* insulin receptor from cDNA libraries from stage 47/48 tadpole brains. Two forms of insulin receptors were identified. Sequence analysis shows that these two *Xenopus* brain insulin receptors are highly similar (94% identical at the nucleotide level and 95% identical at the predicted amino acid level) and are splice variants homologous to a human isoform of insulin receptor lacking exon 11 (Kenner et al., 1995).

We subcloned the more abundant form of insulin receptor into a bidirectional, double-promoter plasmid, in which insulin receptor expression and GFP expression are driven from separate promoters. We predicted that, by electroporating this construct into tectal neurons (Bestman et al., 2006; Haas et al., 2002), we could affect insulin receptor signaling (Figure 2) and identify GFP-labeled tectal neurons for further in vivo structural and functional experiments. Because most if not all insulin receptor signaling requires its kinase activity, we generated a point mutation to abolish insulin receptor binding to ATP. The insulin receptor requires the formation of a disulfide-linked dimer to be a functional receptor (White, 2003). Upon ligand binding, a conformational change that allows intramolecular transphosphorylation is required for the activation of the kinase. Therefore, we expect that the mutated insulin receptor can dimerize with endogenous insulin receptor and function as a dominant-negative receptor by blocking the phosphorylation of endogenous insulin receptor and possibly by sequestering the ligand (Figure 2A). Indeed, several studies have shown that mutation at the ATP-binding site has a dominant-negative effect on insulin-induced functions like glucose uptake by abolishing insulin receptor kinase activity without affecting its binding affinity to insulin (Ebina et al., 1987; Kanezaki et al., 2004).

To evaluate our *Xenopus* insulin receptor constructs, we transfected COS1 cells with wtIR and dnIR tagged with CFP and HA in tandem. The HA tag allows us to perform immunoprecipitation experiments, and the CFP tag allows us to differentiate ectopically expressed from endogenous insulin receptor according to the 27 kD weight shift on western blots. To test whether ectopically expressed dnIR can bind with endogenous insulin receptor and interfere with endogenous insulin receptor activity, we performed immunoprecipitation experiments with the anti-HA antibody. Both wtIR and dnIR coimmunoprecipitate endogenous insulin receptor, indicating that they interact with endogenous insulin receptor (Figure 2B, upper panel). In addition, endogenous insulin receptor that coimmunoprecipitates with wtIR is phosphorylated, but endogenous insulin receptor that coimmunoprecipitates with dnIR is not phosphorylated (Figure 2B, lower panel), even with prolonged exposure of the blot (data not shown). This demonstrates that expression of dnIR blocks phosphorylation of endogenous insulin receptor. For subsequent experiments in this paper, we expressed wtIR and dnIR under the same conditions, i.e., with the same promoter, the same molar concentrations of plasmids, and the same electroporation parameters. Because dnIR only has a point mutation in its ATP-binding site, it retains all the structural properties of the wtIR, except for the kinase activity. The point mutation does not affect the binding affinity of insulin (Ebina et al., 1987), and the dnIR undergoes the same conformational change upon ligand binding as the wtIR (Baron et al., 1992), indicating that both the extracellular domain for ligand binding and the intracellular domain for interaction of receptor dimers is well preserved between dnIR and wtIR. Therefore, we reasoned that expression of the wtIR may serve as a control for nonspecific effects of overexpression of dnIR.

In addition, we obtained a morpholino against a conserved region of both *Xenopus* insulin receptors (moIR) and a morpholino control (moCTRL) containing five mismatches compared to moIR (see Experimental Procedures). moIR reduces expression of *Xenopus* insulin receptor in HEK293 cells compared to moCTRL (Figure 2C). These tools allow us to investigate the role of insulin receptor signaling in neuronal circuit function by insulin receptor knockdown and by dominant-negative inhibition of the insulin receptor activity.

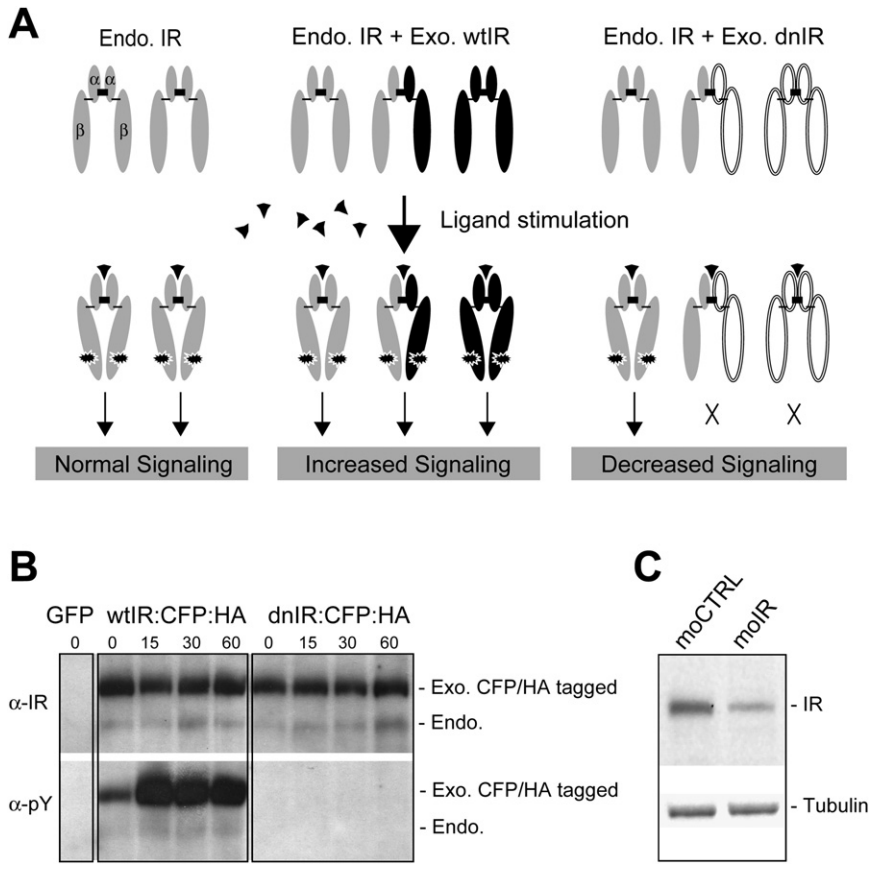

Figure 2. Manipulation of Insulin Receptor Signaling

(A) Model of insulin receptor signaling strength in cells with only endogenous insulin receptor (Endo. IR, left panel) and cells expressing exogenous wtIR (Exo. wtIR, middle panel) or dnIR (Exo. dnIR, right panel). Ectopic expression of wtIR increases total insulin receptor and therefore can increase insulin receptor signaling upon ligand stimulation. The insulin receptor monomer is composed of α, β subunits bridged by an intrinsic disulfide bond (thin, short bar). Two α/β subunits dimerize by an extrinsic disulfide bond (thick, short bar) to generate a functional receptor. Note that exogenous insulin receptor can dimerize with both endogenous and exogenous insulin receptor. Therefore, ectopic expression of dnIR could decrease insulin receptor signaling by blocking the transphosphorylation of insulin receptor heterodimers and possibly by sequestering ligand from endogenous insulin receptor homodimers.

(B) dnIR decreases insulin receptor signaling. COS1 cells were transfected with GFP, wtIR:CFP:HA, or dnIR:CFP:HA. Cells were stimulated with insulin for increasing periods in minutes before immunoprecipitation with the anti-HA antibody. Insulin receptor was detected with anti-IR antibody (top panel). Endogenous COS1 cell insulin receptor is detected in lanes where ectopically expressed *Xenopus* wtIR and dnIR were immunoprecipitated with HA antibody, indicating that ectopic wtIR and dnIR can interact with endogenous COS1 cell insulin receptor. Note that ectopic insulin receptor is shifted upward on the gel by virtue of the CFP. Insulin receptor activation detected by anti-phosphotyrosine antibody (α-pY, bottom panel) shows that wtIR and endogenous co-IP'ed COS1 insulin receptor can be phosphorylated upon insulin stimulation. However, in cells transfected with dnIR, phosphorylation of neither *Xenopus* mutant insulin receptor nor endogenous COS1 insulin receptor can be detected.

(C) moIR decreases insulin receptor protein. Western analysis of insulin receptor in HEK293 cells transfected with *Xenopus* wtIR:CFP:HA followed by moCTRL or moIR. Equal amounts of protein were loaded, as indicated by anti-tubulin antibody (bottom panel). Insulin receptor detected by anti-HA antibody (top panel) shows that ectopically expressed *Xenopus* insulin receptor was decreased with the moIR transfection compared to moCTRL.

Insulin Receptor Signaling Is Critical for Visual Circuit Function

To test whether the insulin receptor is important for circuit function, we record responses to natural light stimuli from tectal neurons in intact animals. We provide tadpoles with a range of light stimuli ranging from relative intensity 10^{-8} to 10^{-1} (see Experimental Procedures) across the entire retina and collect whole-cell recordings from control cells and tectal neurons transfected with GFP, wtIR, or dnIR to record light-evoked compound synaptic currents (CSCs). When a 2.5 s visual stimulus is applied to the eye, neurons in the contralateral optic tectum respond to both the onset and offset of the light stimulus. Because the OFF response is typically larger and more consistent than the ON response, we analyzed the total charge transfer for 1.5 s after the offset of the light stimulus (Figures 3A and 3B). This 1.5 s analysis window was chosen because it is long enough for most if not all responses to return to baseline and short enough to minimize the contamination by spontaneous activity that is independent of visual stimulation. The evoked CSCs, recorded at a holding potential of −70 mV, include direct monosynaptic glutamatergic current and polysynaptic responses integrating inhibitory and excitatory inputs (Engert et al., 2002; Zhang et al., 2000) and serve as a readout for visual circuit function.

Most control neurons do not show evoked responses at the lowest relative intensity of 10^{-8} (Figure 3A). As the light intensity increases, visual stimulation-evoked CSCs increase in magnitude and duration, peaking at 10^{-3} relative intensity before they decrease at relative intensity 10^{-1} (Figures 3A and 3B and Table 1). Because evoked CSCs recorded from GFP-expressing neurons are comparable to nontransfected cells (Table 1), data from nontransfected and GFP-expressing control neurons were pooled for this experiment, and GFP-expressing neurons will be the controls for all following experiments. Visual stimulation-evoked responses in dnIR-expressing tectal neurons are only about half the magnitude of controls (Figures 3A and 3B and Table 1; $p < 0.05$). Analysis of the charge transfer within the initial 50 ms window from the onset of the evoked CSC, which has previously been characterized as predominantly direct excitatory input (Zhang et al., 2000), shows that dnIR-expressing tectal neurons have impaired visual responses compared to controls (Figures 3A and 3D and Table 1; $p < 0.05$). Responses in wtIR-expressing tectal neurons, on the other hand,

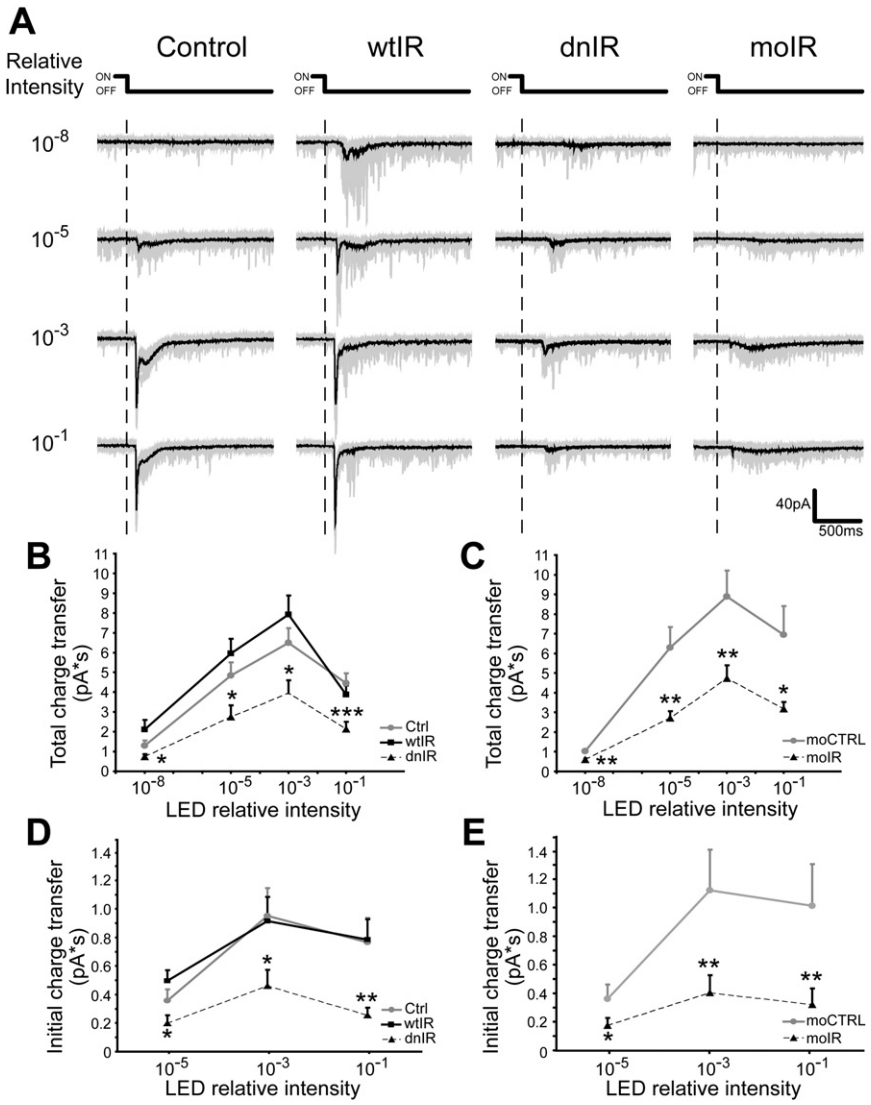

Figure 3. Insulin Receptor Signaling Is Required for Normal Tectal Cell Responses to Visual Input

Whole-cell recordings from tectal neurons in intact tadpoles demonstrate visual stimulation-evoked compound synaptic currents to light OFF responses over a wide range of stimulus intensities. (A) Representative recordings from neurons expressing GFP, wtIR, dnIR, and moIR at different LED intensities. Superimposition of 20 consecutive responses (gray) and the averaged trace (black) are shown.

(B and C) Integrated total charge transfer over the 1.5 s window starting from the decrement of the light. dnIR-expressing tectal neurons (B) and moIR-transfected neurons (C) have significantly smaller visual stimulation-evoked responses than controls and wtIR-expressing cells.

(D and E) Visual stimulation-evoked excitatory responses, defined by integrated initial charge transfer over the 50 ms window starting from the onset the evoked responses, are significantly smaller in dnIR-expressing neurons (D) and moIR-transfected neurons (E) compared to controls, indicating that insulin receptor is required for normal excitatory synaptic function in response to visual inputs. Statistical differences are comparisons between test groups and controls. Data are presented as mean + SEM in (B)–(E).

are not significantly different from controls (Figures 3A, 3B, and 3D and Table 1).

We further assessed the function of the insulin receptor in visual system responses using morpholino-mediated knockdown. We recorded light-evoked responses in tectal neurons transfected with fluorescently labeled moIR or moCTRL. moIR significantly reduced the magnitude of visual responses compared to moCTRL (Figures 3A and 3C and Table 1; $p < 0.05$), and moIR significantly reduced the initial charge transfer compared to moCTRL (Figures 3A and 3E and Table 1; $p < 0.05$). Together, these data indicate that the insulin receptor is critical for excitatory retinotectal transmission in visual circuit function and that defects in insulin receptor signaling caused by dnIR expression are sufficient to cause a reduction in visual responses. It is interesting to note that moIR and dnIR diminish visual responses to a comparable extent, suggesting that the deficient phosphorylation in the dnIR-expressing cells essentially mimics loss of protein. Therefore, we use dnIR in subsequent experiments to probe the mechanism by which the insulin receptor signaling regulates visual system function. In addition, because the responses of tectal neurons expressing wtIR are comparable to controls, expression of wtIR serves to control for potential nonspecific effects caused by overexpression of dnIR.

Insulin Receptor Signaling Regulates Synaptic Transmission

To determine how the insulin receptor affects excitatory input and circuit function, we examined the properties of spontaneous AMPA mEPSC from GFP-, wtIR-, and dnIR-expressing tectal neurons. A change in AMPA mEPSC amplitude usually suggests a change in the number of neurotransmitter receptors at postsynaptic sites, and a change in frequency usually suggests a change in the number of synaptic sites or presynaptic vesicle release probability. The frequency of AMPA mEPSC events in dnIR-expressing tectal neurons is significantly reduced compared to GFP controls (Figures 4A, 4C, and 4D; GFP: 1.06 ± 0.22 Hz, n = 12; dnIR: 0.55 ± 0.16 Hz, n = 18; p = 0.018). wtIR-expressing neurons, however, are not different from GFP controls (Figures 4A, 4C, and 4D; wtIR: 1.16 ± 0.20 Hz, n = 23). In contrast, we find no change in amplitude of AMPA mEPSCs between these three groups, suggesting that ectopic expression of wtIR or dnIR does not change AMPA receptor numbers at the postsynaptic sites (Figures 4B, 4E, and 4F; GFP: 9.76 ± 0.89 pA, n = 12; wtIR: 9.98 ± 0.57 pA, n = 23; dnIR: 8.90 ± 0.54 pA, n = 18). The frequency and amplitude of GABA mIPSC are comparable for all groups of cells (data not shown), suggesting that

Table 1. Charge Transfer of Visual Stimulation Evoked Responses at Different LED Intensity

	Relative Intensity	10^{-8}	10^{-5}	10^{-3}	10^{-1}
Total charge transfer (pA*s)	control	1304 ± 253; n = 13	4846 ± 656; n = 18	6495 ± 748; n=17	4449 ± 511; n = 17
	GFP control	1450 ± 316; n = 10	4618 ± 920; n = 12	6459 ± 822; n = 12	4566 ± 597; n = 12
	NT control	821 ± 133; n = 3	5302 ± 775; n = 6	6580 ± 1777; n = 5	4168 ± 1084; n = 5
	wtIR	2119 ± 483; n = 16	5957 ± 748; n = 16	7925 ± 967; n = 16	3879 ± 467; n = 16
	dnIR	741 ± 133; n = 17 *	2745 ± 602; n = 17 *	3944 ± 655; n = 17 *	2137 ± 366; n = 15 ***
	moCTRL	1020 ± 126; n = 21	6298 ± 1038; n = 21	8884 ± 1327; n = 21	6942 ± 1465; n = 18
	moIR	599 ± 83; n = 22 **	2701 ± 371; n = 22 **	4729 ± 676; n = 21 **	3181 ± 348; n = 20 *
Initial charge transfer (pA*s)	control	-	357 ± 80; n = 17	952 ± 193; n = 17	765 ± 171; n = 17
	GFP control	-	303 ± 88; n = 11	837 ± 219; n = 12	697 ± 195; n = 12
	NT control	-	455 ± 162; n = 6	1230 ± 406; n = 5	929 ± 372; n = 5
	wtIR	-	496 ± 74; n = 16	915 ± 169; n = 16	784 ± 144; n = 16
	dnIR	-	199 ± 56; n = 17 *	459 ± 114; n = 17 *	254 ± 55; n = 15 **
	moCTRL	-	364 ± 99; n = 21	1124 ± 285; n = 21	1031 ± 309; n = 18
	moIR	-	177 ± 53; n = 22 *	406 ± 123; n = 21 **	322 ± 114; n = 20 **

Total charge transfer calculated in a 1.5 s window following the offset of the visual stimulation and initial charge transfer calculated in a 50 ms window following the onset of the evoked response. Responses from GFP control, nontransfected (NT) control, and moCTRL cells are comparable at all intensities tested. Asterisks represent statistical significance between wtIR and dnIR experimental groups and control group that contain data pooled from GFP control and NT control or between the moIR group and moCTRL group.

insulin receptor function specifically affects excitatory synaptic transmission.

To test whether the decrease in AMPA mEPSC frequency reflects a change in presynaptic vesicle release, we applied pairs of stimuli to the optic chiasm and recorded evoked AMPA receptor-mediated synaptic currents from tectal neurons. This paired-pulse protocol has been used widely to examine changes in release probability (Akerman and Cline, 2006; Chen and Regehr, 2003). In tectal neurons expressing GFP, wtIR, and dnIR, the paired-pulse ratios are comparable between these groups, suggesting that insulin receptor signaling in tectal neurons does not retrogradely affect RGC synaptic vesicle release (Figures 5A and 5B; GFP: 2.22 ± 0.25, n = 10; wtIR: 2.23 ± 0.17, n = 14; dnIR: 2.25 ± 0.22, n = 15).

To test whether insulin receptor signaling regulates glutamatergic synaptic maturation, we measured evoked AMPA receptor-mediated and NMDA receptor-mediated responses from GFP-, wtIR-, and dnIR-expressing tectal neurons to determine the AMPA/NMDA ratio, an indicator of synapse maturity (Akerman and Cline, 2006; Wu et al., 1996). We do not detect significant differences in AMPA/NMDA ratio between all groups of cells (Figures 5C and 5D; GFP: 2.86 ± 0.44, n = 21; wtIR: 2.38 ± 0.23, n = 19; dnIR: 2.99 ± 0.31, n = 24) or the fraction of silent synapses (data not shown), indicating that insulin receptor signaling is not necessary for the establishment or maturation of AMPA receptor-mediated synaptic transmission. Together, these results indicate that the insulin receptor does not retrogradely affect presynaptic release probability and is not required for glutamatergic synapse maturation. Therefore, the reduced mEPSC frequency in dnIR-expressing neurons is more likely to result from a reduction in synaptic inputs, consistent with the reduced response to visual stimulation.

Insulin Receptor Signaling Is Required to Maintain Synapse Number

To test whether the reduced visual responses and decreased frequency of spontaneous AMPA mEPSCs are caused by a decrease in synaptic contacts onto dnIR-expressing tectal neurons, we performed electron microscopy to estimate synapse density on tectal neurons. This methodology also provides ultrastructure information about both pre- and postsynaptic profiles, which allows us to evaluate synaptic maturity of tectal neurons. Tadpole brains electroporated with GFP, wtIR, and dnIR constructs were fixed and cut into 60 nm ultrathin sections for transmission electron microscope imaging to identify GFP-positive dendritic profiles. All labeled dendritic profiles with intact membrane structure were imaged under 15,000× magnification, and images were taken approximately every 20 ultrathin sections (~1.2 μm) to avoid oversampling the same synapses. From GFP-, wtIR-, and dnIR-expressing brains, we found 233, 207, and 311 labeled dendritic profiles, which gave total areas of 104.3, 85.3, and 143.9μm^2, respectively. Based on the presence of three criteria—docked presynaptic vesicles, a clear synaptic cleft, and postsynaptic density—we identified 63, 55, and 36 synapses respectively, in the labeled GFP-, wtIR-, or dnIR-expressing dendritic profiles. Synapse density was estimated as the number of labeled synapses normalized to the total labeled dendritic profile area. We found that dnIR-expressing dendrites have less than half of the synapse density of GFP-expressing dendrites (Figure 6B; GFP: 0.60 synapses/μm^2; dnIR: 0.25 synapses/μm^2; $p < 0.0001$, χ^2 test), while wtIR-expressing dendrites have comparable synapse density to controls (Figure 6B; wtIR: 0.64 synapses/μm^2). This result indicates that insulin receptor signaling regulates the establishment or maintenance of synaptic contacts.

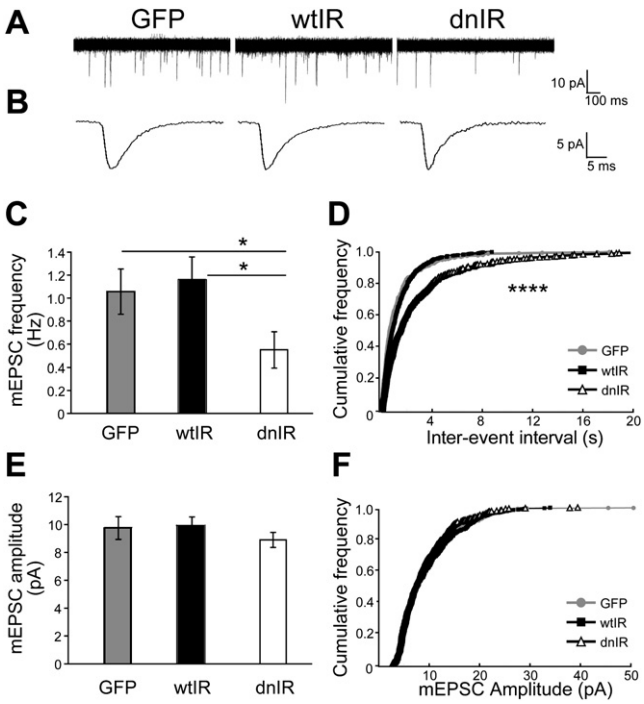

Figure 4. Insulin Receptor Signaling Regulates Frequency of AMPA Receptor-Mediated mEPSC

(A) Representative traces of spontaneous AMPA mEPSCs, superimposed from 30 consecutive traces.

(B) Examples of individual mEPSC.

(C) mEPSC frequency for GFP-, wtIR-, and dnIR-expressing neurons. dnIR-expressing neurons have significantly lower mEPSC frequency compared to GFP controls and wtIR-expressing neurons.

(D) Cumulative distributions of the first 30 inter-mEPSC event intervals. dnIR-expressing neurons have longer interevent intervals than GFP- or wtIR-expressing neurons ($p < 0.0001$, Kolmogorov-Smirnov test). Only event intervals <20 s were plotted, and three data points from dnIR cells with intervals of 22.2, 24.3, and 51.2 s were omitted in this plot.

(E and F) Averaged mEPSC amplitude (E) and cumulative distributions of mEPSC amplitudes from the first 30 mEPSCs (F) for cells expressing GFP, wtIR, and dnIR are comparable.

Data are presented as mean ± SEM in (C) and (E).

To test whether synapse maturity is affected in synapses onto dnIR-expressing neurons, we measured the area of the presynaptic element filled with clustered synaptic vesicles and normalized this value to the area of the presynaptic terminal. Previous data from our lab has shown that, as synapses mature, the relative area of the presynaptic terminal occupied by synaptic vesicles increases, and this value can serve as an index of synapse maturity (Haas et al., 2006). The synapse maturation indices were comparable between GFP, wtIR, and dnIR groups (Figure 6C; GFP: 27.38 ± 2.57; wtIR: 27.69 ± 2.98; dnIR: 28.58 ± 3.20). This result indicates that insulin receptor signaling does not play a role in regulating synapse maturation, consistent with the AMPA/NMDA ratio result previously measured electrophysiologically (Figures 5C and 5D).

To test whether the decrease in synaptic contacts on dnIR-expressing dendrites occurs on all parts of the dendritic tree, and hence is a global effect, or whether insulin receptor signaling preferentially targets, for example, larger-caliber, proximal dendrites or newly formed fine-caliber, distal dendrites, we compared the size of the labeled postsynaptic profile area indicated by its short diameter from GFP-, wtIR-, and dnIR-expressing dendrites (Figure 6D; GFP: 0.65 ± 0.04; wtIR: 0.60 ± 0.03; dnIR: 0.55 ± 0.04). There are no significant differences between these three groups, indicating that the reduction of synapses is a global effect that occurs in all regions of the dendritic tree.

To test whether insulin receptor signaling affects overall dendritic arbor elaboration, we analyzed total dendritic branch length and branch tip number from images of tectal neurons collected at 24 hr intervals over 3 days and found that these parameters for dendritic arbor morphology are comparable between GFP-, wtIR-, and dnIR-expressing cells (see Figure S1 available online).

Insulin Receptor Signaling Regulates Experience-Dependent Structural Plasticity

Insulin receptor signaling could regulate circuit function by affecting experience-dependent structural plasticity. To test whether insulin receptor signaling is required for experience-dependent structural plasticity, we used a protocol in which dendritic arbor growth rates in response to 4 hr of enhanced visual stimulation are compared to growth rates in the absence of visual stimulation (Haas et al., 2006; Sin et al., 2002). Previous work has demonstrated that this visual stimulation protocol enhances dendritic arbor growth rates in tectal neurons by mechanisms that require NMDAR activity, RhoA GTPases, and stabilization of glutamatergic synapses (Haas et al., 2006; Sin et al., 2002). Single neurons expressing GFP alone or GFP with wtIR or dnIR were imaged. Three in vivo images were collected: one before the 4 hr in the dark, a second in between the dark and light periods, and a third after 4 hr of visual stimulation (Figure 7A). Dendritic branch lengths and branch tip behaviors during the dark and the visual stimulation periods were quantified from the 3D reconstructions of arbor structure. In contrast to GFP controls or wtIR-expressing cells, which significantly increase dendritic growth rates in response to visual stimulation (Figures 7A and 7B; GFP: Dark/Light: 66.18 ± 8.60/124.36 ± 15.71 μm per 4 hr, n = 11, p = 0.016, Wilcoxon test; wtIR: Dark/Light: 81.46 ± 14.79/124.97 ± 20.06 μm per 4 hr, n = 11, p = 0.013, Wilcoxon test), dnIR-expressing neurons fail to increase their growth rates in response to visual stimulation (Figures 7A and 7B; Dark/Light: 106.81 ± 11.36/105.25 ± 14.88 μm per 4 hr, n = 11). These results indicate that insulin receptor signaling is required for increases in dendritic arbor growth rates in tectal neurons normally seen with visual stimulation.

Dendritic arbor branches are dynamic over time periods of minutes to hours, with branches being constantly added and lost, extended and retracted. The change in growth rates between the dark and visual stimulation periods could result from changes in the relative distribution of dynamic branch behaviors such as branch length retraction and extension and/or branch tip loss and addition, because each of these events reflects different cellular and molecular mechanisms (Sin et al., 2002). We tracked individual terminal branches through the dark and visual stimulation periods to determine the behavior of each branch. For branch length analysis, we found that GFP- and wtIR-expressing

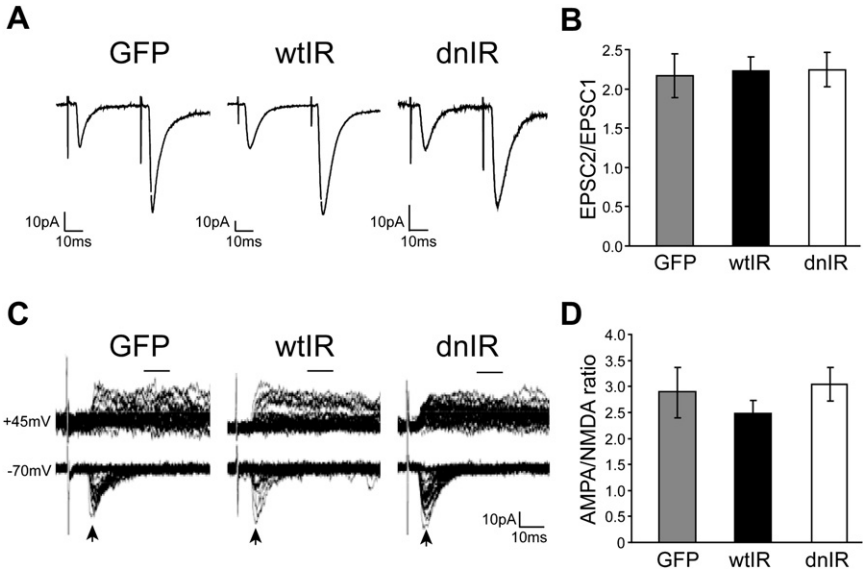

Figure 5. Insulin Receptor Signaling Does Not Alter Presynaptic Vesicle Release Probability or Electrophysiological Synapse Maturation

(A) Representative traces of evoked monosynaptic EPSCs in response to pairs of stimuli.

(B) Paired-pulse ratio, defined as the ratio of peak AMPA amplitudes (EPSC2/EPCS1), is not different between GFP-, wtIR-, and dnIR-expressing neurons.

(C) Overlays of 30 consecutive sample traces recorded at −70 mV and +45 mV in response to RGC axon stimulation. Arrows and bars show where AMPA and NMDA currents were measured.

(D) AMPA/NMDA ratio is comparable between GFP-, wtIR-, and dnIR-expressing cells.

Data are presented as mean ± SEM in (B) and (D).

cells have similar rates of branch retraction in the dark and visual stimulation periods (Figure 7C; GFP: Dark/Light: 141.15 ± 6.24/147.16 ± 11.22 μm per 4 hr; wtIR: Dark/Light: 167.11 ± 23.85/171.49 ± 22.36 μm per 4 hr). In contrast, dnIR-expressing cells show significantly higher retraction rates during visual stimulation (Figure 7C; Dark/Light: 182.83 ± 17.51/210.51 ± 15.39 μm per 4 hr, p = 0.041, Wilcoxon test). Both GFP and wtIR-expressing cells show increased branch length extension during the visual stimulation period (Figure 7C; GFP: Dark/Light: 206.88 ± 12.65/266.86 ± 17.15 μm per 4 hr, p = 0.013; wtIR: Dark/Light: 248.73 ± 30.08/296.12 ± 34.18 μm per 4 hr, p = 0.021, Wilcoxon test). However, dnIR-expressing cells do not show an increase in branch length extension during visual stimulation (Figure 7C, right; Dark/Light: 289.64 ± 18.80/315.40 ± 18.46 μm per 4 hr).

For branch tip analysis, we categorized each branch as stable, lost, or added based on its presence before and after the dark or visual stimulation period (Figure 7D). GFP-, wtIR-, and dnIR-expressing cells all increase stable branches during visual stimulation (Figure 7E; GFP: Dark/Light: 41.55 ± 6.47/55.45 ± 8.88,

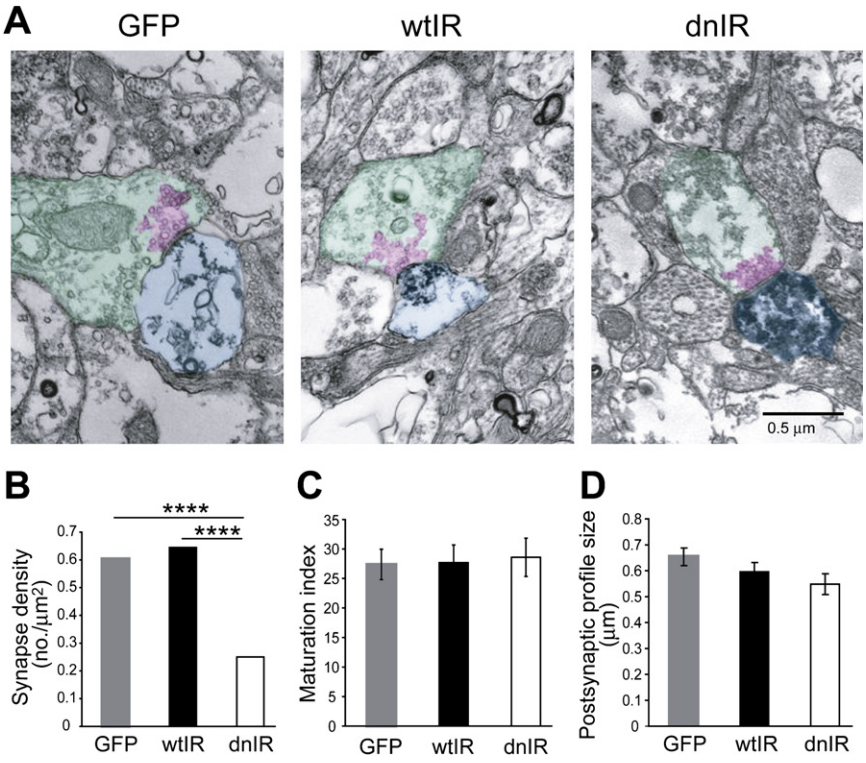

Figure 6. Insulin Receptor Regulates Synapse Numbers

(A) Electron micrographs show ultrastructural morphology of synaptic terminals that contact GFP-, wtIR-, and dnIR-expressing dendrites. Postsynaptic areas, presynaptic area, and the clustered synaptic vesicle were highlighted in light blue, green, and pink, respectively.

(B) dnIR-expressing dendrites receive significantly fewer synapse contacts compared to GFP- and wtIR-transfected dendrites.

(C) Synapses that contact GFP-, wtIR-, and dnIR-expressing dendrites show comparable ultrastructural synaptic maturity, determined by the area occupied by clustered synaptic vesicles relative to the area of the presynaptic terminal.

(D) GFP-, wtIR-, and dnIR-expressing neurons have comparable ranges of postsynaptic profile sizes, represented by the short diameter of labeled postsynaptic area.

Data are presented as mean ± SEM in (C) and (D).

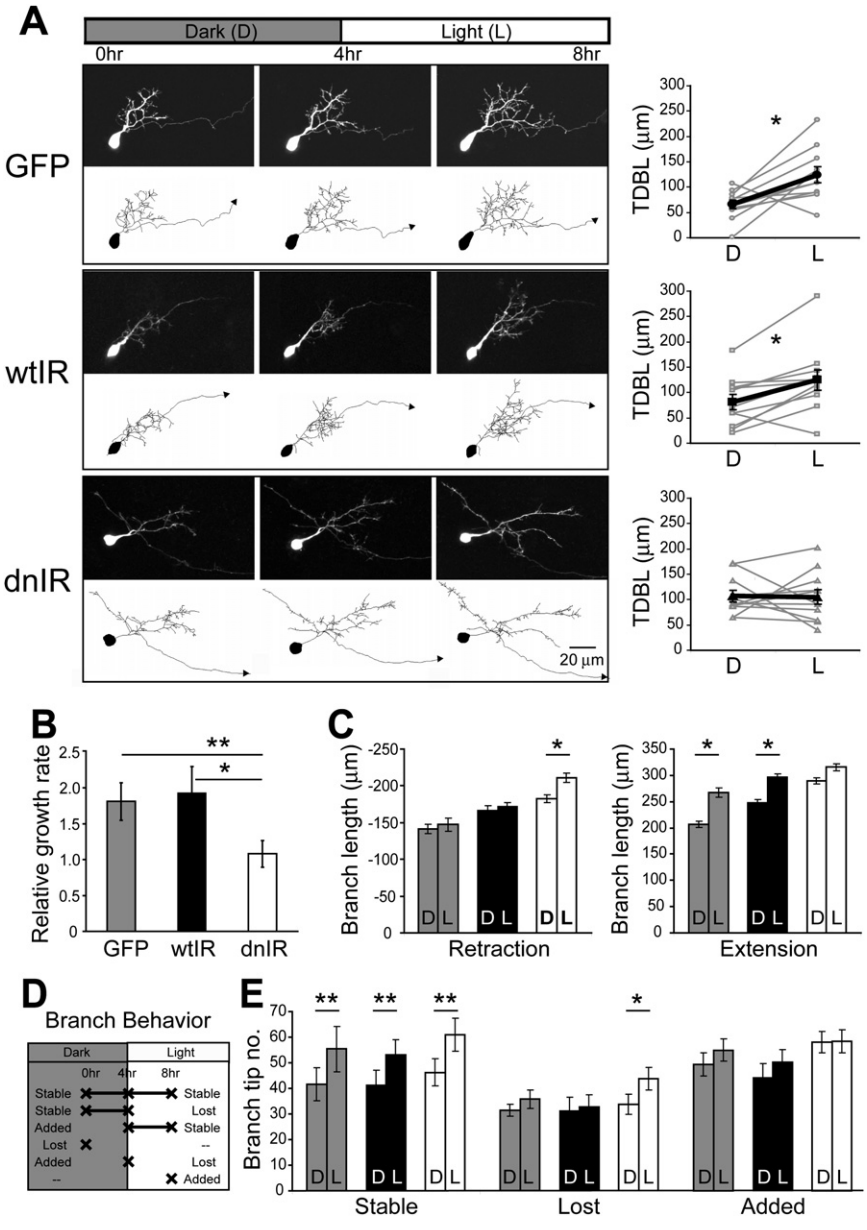

Figure 7. Insulin Receptor Signaling Modulates Experience-Dependent Dendritic Structural Plasticity

(A) (Top) Schematic of the visual stimulation protocol. In vivo time-lapse images were collected before and after animals were exposed to 4 hr of dark and 4 hr of enhanced visual stimulation. Images and 3D reconstructions of representative neurons are shown for each group. Growth rates for individual neurons (gray) with the mean ± SEM (black) are shown on the right panel. GFP- and wtIR-expressing neurons significantly increase arbor growth rates with visual stimulation, whereas dnIR-expressing neurons do not increase growth rates in response to visual stimulation.

(B) Dendritic arbor growth rates seen with visual stimulation normalized to the growth rate in the dark. GFP- and wtIR-expressing cells double their growth rate during the visual stimulation period, whereas dnIR-expressing neurons do not respond to visual stimulation and have significantly reduced relative growth rates compared to GFP- and wtIR-expressing neurons.

(C) Branch length retraction and extension of existing branches during the dark and visual stimulation periods. GFP- and wtIR-expressing neurons retract branch length at the same rate in the dark and with visual stimulation, but extend significantly more branch length during the visual stimulation period. dnIR-expressing neurons retract significantly more branch length and fail to increase branch extensions with the visual stimulation.

(D) Classification of individual branch tips into stable, lost, and added dynamic branch categories during the dark and visual stimulation periods.

(E) Number of stable, lost, and added branch tips during the dark and visual stimulation periods. All groups of neurons have more stable branches with visual stimulation than in the dark, and they have comparable numbers of added branches during the visual stimulation period compared to the dark period. However, dnIR-expressing neurons lost significantly more branches during the visual stimulation treatment, while other groups have the same rates of branch tip loss in the dark or with visual stimulation. TDBL, total dendritic branch length.

Data are presented as mean ± SEM in (B), (C), and (E).

p = 0.008; wtIR: Dark/Light: 41.36 ± 5.87/53.09 ± 5.93, p = 0.005; dnIR: Dark/Light: 46.27 ± 5.41/61.00 ± 6.40, p = 0.003; Wilcoxon test) and have similar rates of branch addition during the dark and visual stimulation periods (Figure 7E; GFP: Dark/Light: 49.36 ± 4.46/55.00 ± 4.45; wtIR: Dark/Light: 44.18 ± 5.34/50.18 ± 5.00; dnIR: Dark/Light: 58.00 ± 4.27/58.45 ± 4.50). However, while GFP and wtIR cells show the same degree of branch tip loss during the dark and visual stimulation periods (Figure 7E; GFP: Dark/Light:31.09 ± 2.39/35.45 ± 3.56; wtIR: Dark/Light: 30.82 ± 5.29/32.45 ± 4.63), dnIR-expressing neurons lose significantly more branches over the 4 hr visual stimulation period (Figure 7E; Dark/Light: 33.36 ± 3.95/43.27 ± 4.42, p = 0.026, Wilcoxon test). Together, these data indicate that insulin receptor signaling promotes dendritic arbor elaboration by increasing branch length extension and by decreasing branch retraction and branch tip loss in an experience-dependent manner.

DISCUSSION

Synaptic connectivity is dynamic and determined by a balance between synapse formation and elimination that continues throughout development into adulthood (Trachtenberg et al., 2002). By taking advantage of the *Xenopus* visual circuit as an in vivo experimental system amenable to molecular manipulation, electrophysiology, and a variety of imaging methods, we show that the insulin receptor is required for optic tectal neurons to receive normal levels of visual input within the retinotectal circuit. Deficits in insulin receptor signaling severely dampen

glutamatergic synaptic transmission as shown by reduced AMPA mEPSC frequency and the reduction in visually evoked synaptic currents in dnIR-expressing tectal neurons. Ultrastructural studies demonstrate that these effects are caused by a reduction in synaptic contacts onto tectal neurons. Furthermore, we show that decreased insulin receptor signaling prevents experience-dependent increases in dendritic arbor growth rates normally seen with visual stimulation (Haas et al., 2006; Sin et al., 2002). Together, these data demonstrate that insulin receptor signaling plays crucial roles in circuit function by regulating synapse density, synaptic transmission, experience-dependent dendritic structural plasticity, and response to afferent inputs within a circuit. These diverse outcomes of reduced insulin receptor function may all originate from a vital role for insulin receptor signaling in the maintenance of excitatory synapses.

Cell-Autonomous Role of Insulin Receptor Signaling in the CNS

Although the brain had been conventionally considered as an insulin-insensitive organ, emerging data suggest a role for insulin and insulin receptor signaling in the CNS. Several studies have shown that relatively brief exposure to insulin accelerates transmitter receptor trafficking to the plasma membrane (Passafaro et al., 2001; Skeberdis et al., 2001; Wan et al., 1997); however, the same insulin treatment has been shown to induce receptor endocytosis and decrease synaptic strength (Ahmadian et al., 2004; Beattie et al., 2000; Man et al., 2000). An increased understanding of insulin receptor signaling in the brain would benefit from the tools to control receptor activity and manipulate its postulated function in vivo. Transgenic studies using mutant insulin receptors have demonstrated a role for insulin receptor signaling, for example, in axon guidance in flies (Song et al., 2003). However, like direct insulin treatment, system-wide insulin receptor perturbation lacks the desired spatial or temporal resolution. In addition, prolonged insulin receptor perturbation through the transgenic strategy might result in compensatory effects in the system. To address these potential problems, we developed tools to manipulate endogenous insulin receptor signaling at the single-cell level to study the physiological function of insulin receptor signaling in vivo. Knowing that the insulin receptor is widely distributed in the visual circuit of *Xenopus* tadpoles (Figure 1), we electroporated wtIR, dnIR constructs, or morpholinos to alter insulin receptor signaling in single optic tectal neurons in an otherwise unaltered environment.

To assess the role of insulin receptor signaling in circuit function, we recorded responses to natural light stimuli over a range of light intensities from transfected optic tectal neurons. dnIR-expressing or moIR-transfected neurons respond very poorly to every light intensity tested, indicating that insulin receptor signaling is required for tectal neurons to receive normal levels of visual input (Figure 3). Despite biochemical evidence that wtIR increases insulin receptor signaling in COS cells (data not shown), we do not detect statistically significance increases in visual responses in wtIR-expressing neurons. Possible explanations for this are that the ligand, receptor, or downstream signaling pathways may be either saturated or rate limiting in order to protect cells from overactive insulin receptor signaling.

Insulin Receptor Signaling and Experience-Dependent Dendritic Plasticity

Activity shapes synaptic connectivity and dendritic morphogenesis in the CNS, particularly in sensory regions. We have previously demonstrated that visual experience promotes tectal neuron dendritic arbor growth rate (Sin et al., 2002). Here, we show that insulin receptor signaling plays a role in experience-dependent structural plasticity. In addition, we dissected the cellular mechanisms for visual stimulation-induced increases in dendritic arbor growth by identifying changes in individual dendritic branch dynamics during 4 hr periods in the dark or with visual stimulation. Enhanced visual stimulation induces control tectal neurons to increase their rate of dendritic growth by increasing branch length extension and branch tip stabilization. In the absence of insulin receptor signaling, more branches shorten and more branches are lost during the period of visual stimulation. These observations, together with the reduced synapse density in dnIR-expressing neurons, suggest that insulin receptor signaling maintains both synapses and branches which in turn promotes dendritic branch extension with visual experience. These data are consistent with the synaptotrophic hypothesis, which states that the formation and maintenance of synapses promote the stabilization of dendritic branches and that dendritic growth correlates positively with the number and strength of synapses. In the optic tectum of *Xenopus*, visual experience increases dendritic arbor growth rate, retinotectal synaptogenesis, and retinotectal synaptic strength (Aizenman and Cline, 2007; Haas et al., 2006; Sin et al., 2002; Zhang et al., 2000). Similarly, in zebrafish, synapses appear to stabilize growing dendrites and promote further dendrite branch growth in tectal neurons (Niell et al., 2004). Conversely, blocking synapse maturation by interfering with AMPAR trafficking into synapses reduces dendritic arbor elaboration and completely blocks the visual stimulation-induced increase in dendritic arbor growth (Haas et al., 2006). Therefore, the visual stimulation-induced increase in synapse number and strength (Aizenman and Cline, 2007) appears to stabilize newly extended dendritic branches. The failure of dnIR-expressing neurons to increase their growth rate in response to visual stimulation could be a result of their low synapse density. One potential mechanism by which a lower synapse density could affect experience-dependent structural plasticity is that dnIR-expressing neurons do not form and maintain synapses on newly added branches, and they are consequently retracted. The alternate, but not mutually exclusive, mechanism is based on the fact that, in these experiments, we transfected single tectal neurons within an otherwise normal optic tectum. Therefore, while surrounding tectal cells, which have twice the synapse density of the dnIR cell, respond to visual stimulation normally and can increase their synapses and promote dendritic growth, the single dnIR-expressing neuron, which responds to visual inputs very weakly, may not be able to compete with normal neighboring tectal neurons for retinal inputs. Consequently, this might lead to branch length retraction and branch loss in the dnIR-expressing neurons.

Insulin Receptor Signaling and Synaptic Function

The decrease in synapse density, AMPA mEPSCs, and visual responses are consistent with the findings suggesting that insulin

receptor signaling can increase excitatory synapse function. Insulin reportedly stimulates postsynaptic density-95 (PSD-95) protein expression through PI3K-Akt-mammalian target of rapamycin signaling in hippocampus slices and synaptosomes (Lee et al., 2005). In addition, several molecules downstream of the insulin receptor have been implicated in excitatory synaptic connectivity and dendritic structure. For instance, IRSp53, an insulin receptor substrate enriched in the brain, where it localizes to synapses as a component of the postsynaptic density (PSD; Abbott et al., 1999), is particularly interesting. Overexpression of IRSp53 in cultured hippocampal neurons can increase spine density, whereas RNAi knockdown of IRSp53 protein decreases spine density (Choi et al., 2005). Biochemical studies show that IRSp53 directly interacts with PSD scaffold proteins, Shank and PSD-95, small GTPases, such as Rac and Cdc42, and actin regulators, such as WAVE2 and Mena (Choi et al., 2005; Govind et al., 2001; Krugmann et al., 2001; Miki et al., 2000; Soltau et al., 2002). These data suggest a link between insulin receptor signaling and the structural stabilization of excitatory synaptic contacts through the association of synaptic scaffolding proteins and the cytoskeleton and are consistent with our previous studies showing that the small GTPases, Rac and RhoA, operate downstream of glutamate receptors in tectal neurons to mediate visual experience-dependent structural plasticity (Sin et al., 2002). Aside from reports on insulin treatments increasing GABA receptor trafficking from Wang's group (Wan et al., 1997), most studies have shown an effect of insulin signaling on excitatory connections. Consistent with this, our data show no significant difference in spontaneous GABA mIPSC events, indicating that insulin receptor signaling could have a specific function at excitatory synapses. Together, the data suggest that insulin receptor signaling specifically regulates excitatory synaptic inputs in a variety of experimental systems, possibly mediated by cytoskeletal rearrangements.

It is interesting to note that dendritic elaboration can still occur over a period of several days, even when synapse density is low. A similar observation was reported with manipulation levels of the neurotrophin BDNF, which significantly changed synapse number but not dendritic arbor morphology (Sanchez et al., 2006). In the case of insulin receptor signaling where experience-dependent structural plasticity is decreased when assayed over a period of 4 hr, these daily imaging data suggest that, under conditions of decreased synaptic input, alternative mechanisms participate in dendritic arbor growth control.

In conclusion, our data suggest that insulin receptor signaling maintains synapse density and further support the idea that the synapse loss seen with impaired insulin receptor signaling decreases experience-dependent plasticity and ultimately leads to deficits in circuit function, including information processing and integration.

EXPERIMENTAL PROCEDURES

Animals

Albino *X. laevis* tadpoles obtained from lab colony or commercial sources (Nasco, Fort Atkinson, WI) were reared in a 12 hr light/12 hr dark cycle incubator. Stage 47/48 tadpoles (Nieuwkoop and Faber, 1956) were used for all experiments.

Immunohistochemistry

Xenopus tadpoles were anesthetized with 0.02% MS222 (3-aminobenzoic acid ethyl ester), fixed with 4% paraformaldehyde (Electron Microscopy Sciences, Fort Washington, PA) in PBS followed by cryoprotection in 30% sucrose. Whole heads were cut into 25 μm horizontal cryosections. Sections were blocked in 10% goat serum and 0.3% Triton X-100 in PBS for 1 hr before incubating overnight at 4°C in anti-insulin receptor β antibody (αIRβ; Upstate/Millipore, Lake Placid, NY). After washing with Tris-buffered saline (50 mM Tris-HCl, 150 mM NaCl, and 0.1% Tween-20, pH 7.4), sections were incubated in Alexa Fluor 488 conjugated anti-rabbit secondary antibody (Molecular Probes/Invitrogen, Eugene, OR) for 1 hr. Sections were mounted in Vectashield (Vector Laboratories, Burlingame, CA) and imaged with a Zeiss LSM 510 Meta confocal microscope (Carl Zeiss, Jena, Germany). All chemicals were obtained from Sigma-Aldrich (St. Louis, MO) unless otherwise stated.

Plasmids and Morpholinos

The *X. laevis* cDNAs for two forms of the insulin receptor were cloned from 5′ and 3′ RACE cDNA libraries made by the SMART RACE cDNA Amplification kit (Clontech Laboratories, Mountain View, CA) according to the manufacturer's protocol. To knock down both isoforms of the insulin receptor, we obtained a morpholino against a conserved region of both *Xenopus* insulin receptors (moIR; CCCCTCAA TACACCCTGTCCCATGC) and a control morpholino containing five mismatched sites (moCTRL; CCgCTCAtTACACgCTcTCCgATGC) from Gene Tools (Philomath, OR). Both morpholinos are fluorescein tagged so that we can identify morpholino-transfected neurons in vivo. In addition, cDNA of the more abundant insulin receptor isoform was inserted into a bidirectional PCS2 vector consisting of two CMV promoters to express eGFP (Clontech Laboratories) from one strand and either wtIR, dnIR, or nothing from the other strand. The dnIR is a point mutation generated by replacing the lysine residue at position 1058 of the insulin receptor with a methonine residue by the QuickChange XL Site-Direct Mutagenesis Kit (Stratagene, La Jolla, CA) and confirmed with DNA sequencing.

Immunoprecipitation and Western Blot Analysis

COS1 cells were cultured in Dulbecco's modified Eagle's medium (DMEM) supplemented with 10% fetal bovine serum and transfected with FuGENE 6 (Roche Applied Science, Indianapolis, IN) with the double promoter constructs expressing GFP alone or with fusion proteins of wtIR:CFP:HA and dnIR:CFP:HA for 2 days. Cells were then incubated in serum-free DMEM overnight followed by 0.1 μM bovine insulin stimulation and immediately lysed in ice-cold RIPA buffer (50 mM Tris-Hcl, 150 mM NaCl, 1% NP-40, 10 mM NaF, 0.1% SDS, pH 7.4) containing a protease inhibitor cocktail tablet (Roche Applied Science) and 1 mM sodium orthovanadate. An equal amount of total protein from each group of cells was subject to immunoprecipitation with anti-HA antibody (Covance, Emeryville, CA) followed by a western blot analysis with anti-phosphotyrosine antibody (α-PY; BD Biosciences, San Jose, CA). Blots were stripped and reprobed with anti-IRβ (Santa Cruz Biotechnology, Santa Cruz, CA). For morpholino experiments, HEK293 cells were cultured and transfected as described above. 12–16 hr after transfection of GFP, wtIR:CFP:HA and dnIR:CFP:HA, moIR and moCTRL morpholinos were introduced by Endo-Porter (Gene Tools) according to the manufacturer's protocol. Cells were harvested 2 days after the delivery of morpholinos for western blot analysis with the anti-HA and anti-tubulin (Santa Cruz Biotechnology) antibodies.

Neuronal Transfection

For electrophysiology or electron microscopy experiments, bulk tectal neuron transfections were accomplished by electroporation (Haas et al., 2002) of DNA plasmids (0.68 μM) or morpholinos (500 μM). This method transfected ~3%–10% of neurons for plasmids and ~20% of cells for morpholinos in the tectum. Experiments were done at stage 47/48, 3 days after electroporation. For in vivo imaging experiments, individual optic tectal neurons were transfected by single-cell electroporation (Bestman et al., 2006). Only tadpoles with single transfected tectal neurons were selected for time-lapse imaging.

Electrophysiology

For in vivo visual circuit analysis, transfected tadpoles were anesthetized and transferred to HEPES-buffered extracellular solution (115 mM NaCl, 4 mM KCl, 3 mM $CaCl_2$, 3 mM $MgCl_2$, 5 mM HEPES, 10 mM glucose, 10 μM glycine,

pH 7.2 with NaOH, osmolality 255 mOsm) containing 0.25 mM tubocurarine to prevent muscle contraction. After peeling off the skin to expose the brain and cutting along the dorsal midline to expose the cell bodies, tadpoles were transferred into a chamber stabilized with fine tungsten wire (California Fine Wire, Grover Beach, CA) and perfused with extracellular solution with tubocurarine. Visual stimuli were delivered with a green LED pigtailed to a fiber (530 nm Luxon III LED and 2 mm fiberoptic, Doric Lenses, Quebec) opposed to the eye so that it covers the full field of the eye. The LED intensity was controlled with neutral density filters (Oz Optics, Ontario) that dropped into a housing coupled to the fiber. The radiance flux output of the fiber measured by an IL1400 radiometer/photometer (International Light Technologies, Peabody, MA) ranged from 3×10^{-8} to 3×10^{-1} mW and is referred to as relative intensity 10^{-8} to 10^{-1}. Whole-cell recording at −70 mV holding potential was performed at room temperature (21°C–23°C) using glass micropipettes (6–10 MΩ) filled with intracellular saline I (100 mM potassium gluconate, 8 mM KCl, 5 mM NaCl, 1.5 mM $MgCl_2$, 20 mM HEPES, 10 mM EGTA, 2 mM ATP, 0.3 mM GTP, pH 7.2 with KOH, osmolality 255 mOsm). The visual stimulus protocol consists of a light adaptation period (100 s of 2.5 ms pulses at 200 Hz, which gives the effective intensity equal to 50% of the stimulus intensity) and a light stimulus (100 s of 2.5 s pulses at 0.2 Hz). The stimulus protocol was repeated four times from the lowest to the highest intensity while recording from optic tectal neurons counterlateral to the stimulated eye.

For spontaneous AMPA mEPSC, brains were isolated for whole-cell recording (Wu et al., 1996). Recordings were done at −70 mV, and the extracellular solution contained 1 μM tetrodotoxin (Alomone Labs, Jerusalem, Israel) and 100 μM picotoxin (Tocris Biosciences, Ellisville, MO) and the internal solution II (80 mM cesium methanesulfonate, 5 mM $MgCl_2$, 20 mM tetraethylammonium chloride, 10 mM EGTA, 20 mM HEPES, 2 mM ATP, 0.3 mM GTP, pH 7.2 with CsOH, osmolality 255 mOsm) was used. 3–5 min of recording were analyzed from each cell, and mEPSCs were detected with a template-matching algorithm using Axograph 4.6.

For electrical stimulation experiments, a bipolar stimulating electrode (Frederick Haer Company, Bowdoinham, ME) was placed in the optic chiasm to activate RGC axons that innervate the tectum. The stimulus intensity was set to elicit transmission from a single or a few retinal axons onto the monitored postsynaptic tectal neurons, so-called minimal stimulation (Wu et al., 1996). Evoked monosynaptic AMPA receptor-mediated currents were recorded with intracellular solution I at −70 mV, and NMDA receptor-mediated currents were recorded at +45 mV. The AMPA/NMDA ratio was calculated from peak AMPA amplitudes from the non-failure events divided by non-failure NMDA amplitude averaged from 10 ms window, positioned 20 ms after the AMPA peak. The fraction of silent (NMDAR-only) synapses was determined as described (Wu et al., 1996). For the paired-pulse ratio experiment, pairs of stimuli (25 Hz, 25–50 trials) were delivered, and the ratio was calculated as the peak AMPA amplitude ratio (EPSC2/EPSC1).

Upon entering whole-cell mode, we allowed 5 min for dialysis of the intracellular solution before collecting data. All reported voltages were corrected for the liquid junction potential. Neurons had input resistances in a range of 1–4 GΩ and series resistances <100 MΩ, which were monitored throughout the experiments. Signals were measured with Axopatch 200B amplifier and digitized using a Digidata 1322A analog-to-digital board. Stimulation and data acquisition were performed with pClamp 8.0 software and digitized at 10 kHz. Data were analyzed using Axograph 4.6 or Clampfit 10.0 software. All equipment and software are from Axon Instruments/Molecular Devices.

Electron Microscopy

Tadpoles were fixed in 3.5% paraformaldehyde and 0.25% glutaraldehyde (Electron Microscopy Sciences) for 2.5 hr and processed as described in Haas et al. (2006). The optic tectum containing GFP immunoreactivity was cut into 60 nm ultrathin sections, which were collected on pioloform-coated nickel slot grids (Ted Pella, Redding, CA) for examining on a Hitachi 7500 electron microscope (Tokyo, Japan). NIH Image J was used for analysis of size of dendritic, presynaptic, and postsynaptic profiles. Results were from three independent experiments.

In Vivo Imaging and Morphometric Analysis

One day after single-cell electroporation, tadpoles were screened for individually transfected tectal neurons in which every individual branch could be identified (TDBL less than ~1000 μm). Tectal neurons were imaged in vivo using a custom-designed two-photon microscope as described in Haas et al. (2006). Images were collect by Olympus Fluoview software (Tokyo, Japan) at 2× zoom and 1.5 μm step-size in z axis to capture the entire extent of the dendritic arbor. 3D reconstructions of dendritic arbors were done manually by using Object Image software with custom macros (Ruthazer and Cline, 2002). All treatment, imaging, and 3D reconstruction procedures are done blind to avoid biases.

Statistical Tests

Data were tested with the nonparametric Mann-Whitney test to compare between groups unless otherwise stated. Data are presented as mean ± SEM. Significance were labeled as *p < 0.05, **p < 0.01, ***p < 0.001, and ****p < 0.0001.

SUPPLEMENTAL DATA

The Supplemental Data for this article can be found online at http://www.neuron.org/cgi/content/full/58/5/708/DC1/.

ACKNOWLEDGMENTS

We thank Jay Demas for help with the visual stimulation setup, Jianli Li and Kimberly Bronson for assistance with the electron microscopy, and Kimberly Bronson for preparing the cryosections. We also thank members of the Cline laboratory for helpful discussions. This research was support by the National Eye Institute (H.T.C) and Elisabeth Sloan Livingston Foundation Fellowship (S.-L.C).

Received: October 5, 2007
Revised: March 26, 2008
Accepted: April 16, 2008
Published: June 11, 2008

REFERENCES

Abbott, M.A., Wells, D.G., and Fallon, J.R. (1999). The insulin receptor tyrosine kinase substrate p58/53 and the insulin receptor are components of CNS synapses. J. Neurosci. *19*, 7300–7308.

Ahmadian, G., Ju, W., Liu, L., Wyszynski, M., Lee, S.H., Dunah, A.W., Taghibiglou, C., Wang, Y., Lu, J., Wong, T.P., et al. (2004). Tyrosine phosphorylation of GluR2 is required for insulin-stimulated AMPA receptor endocytosis and LTD. EMBO J. *23*, 1040–1050.

Aizenman, C.D., and Cline, H.T. (2007). Enhanced visual activity in vivo forms nascent synapses in the developing retinotectal projection. J. Neurophysiol. *97*, 2949–2957.

Akerman, C.J., and Cline, H.T. (2006). Depolarizing GABAergic conductances regulate the balance of excitation to inhibition in the developing retinotectal circuit in vivo. J. Neurosci. *26*, 5117–5130.

Baron, V., Kaliman, P., Gautier, N., and Van Obberghen, E. (1992). The insulin receptor activation process involves localized conformational changes. J. Biol. Chem. *267*, 23290–23294.

Beattie, E.C., Carroll, R.C., Yu, X., Morishita, W., Yasuda, H., von Zastrow, M., and Malenka, R.C. (2000). Regulation of AMPA receptor endocytosis by a signaling mechanism shared with LTD. Nat. Neurosci. *3*, 1291–1300.

Bestman, J.E., Ewald, R.C., Chiu, S.L., and Cline, H.T. (2006). In vivo single-cell electroporation for transfer of DNA and macromolecules. Nat. Protoc. *1*, 1267–1272.

Chen, C., and Regehr, W.G. (2003). Presynaptic modulation of the retinogeniculate synapse. J. Neurosci. *23*, 3130–3135.

Choi, J., Ko, J., Racz, B., Burette, A., Lee, J.R., Kim, S., Na, M., Lee, H.W., Kim, K., Weinberg, R.J., and Kim, E. (2005). Regulation of dendritic spine morphogenesis by insulin receptor substrate 53, a downstream effector of Rac1 and Cdc42 small GTPases. J. Neurosci. *25*, 869–879.

Clarke, D.W., Mudd, L., Boyd, F.T., Jr., Fields, M., and Raizada, M.K. (1986). Insulin is released from rat brain neuronal cells in culture. J. Neurochem. *47*, 831–836.

Cline, H.T., Wu, G.Y., and Malinow, R. (1996). In vivo development of neuronal structure and function. Cold Spring Harb. Symp. Quant. Biol. *61*, 95–104.

Dou, J.T., Chen, M., Dufour, F., Alkon, D.L., and Zhao, W.Q. (2005). Insulin receptor signaling in long-term memory consolidation following spatial learning. Learn. Mem. *12*, 646–655.

Ebina, Y., Araki, E., Taira, M., Shimada, F., Mori, M., Craik, C.S., Siddle, K., Pierce, S.B., Roth, R.A., and Rutter, W.J. (1987). Replacement of lysine residue 1030 in the putative ATP-binding region of the insulin receptor abolishes insulin- and antibody-stimulated glucose uptake and receptor kinase activity. Proc. Natl. Acad. Sci. USA *84*, 704–708.

Engert, F., Tao, H.W., Zhang, L.I., and Poo, M.M. (2002). Moving visual stimuli rapidly induce direction sensitivity of developing tectal neurons. Nature *419*, 470–475.

Govind, S., Kozma, R., Monfries, C., Lim, L., and Ahmed, S. (2001). Cdc42Hs facilitates cytoskeletal reorganization and neurite outgrowth by localizing the 58-kD insulin receptor substrate to filamentous actin. J. Cell Biol. *152*, 579–594.

Haas, K., Jensen, K., Sin, W.C., Foa, L., and Cline, H.T. (2002). Targeted electroporation in Xenopus tadpoles in vivo—from single cells to the entire brain. Differentiation *70*, 148–154.

Haas, K., Li, J., and Cline, H.T. (2006). AMPA receptors regulate experience-dependent dendritic arbor growth in vivo. Proc. Natl. Acad. Sci. USA *103*, 12127–12131.

Havrankova, J., Roth, J., and Brownstein, M. (1978). Insulin receptors are widely distributed in the central nervous system of the rat. Nature *272*, 827–829.

Hori, K., Yasuda, H., Konno, D., Maruoka, H., Tsumoto, T., and Sobue, K. (2005). NMDA receptor-dependent synaptic translocation of insulin receptor substrate p53 via protein kinase C signaling. J. Neurosci. *25*, 2670–2681.

Kanezaki, Y., Obata, T., Matsushima, R., Minami, A., Yuasa, T., Kishi, K., Bando, Y., Uehara, H., Izumi, K., Mitani, T., et al. (2004). K(ATP) channel knockout mice crossbred with transgenic mice expressing a dominant-negative form of human insulin receptor have glucose intolerance but not diabetes. Endocr. J. *51*, 133–144.

Kenner, K.A., Kusari, J., and Heidenreich, K.A. (1995). cDNA sequence analysis of the human brain insulin receptor. Biochem. Biophys. Res. Commun. *217*, 304–312.

Krugmann, S., Jordens, I., Gevaert, K., Driessens, M., Vandekerckhove, J., and Hall, A. (2001). Cdc42 induces filopodia by promoting the formation of an IRSp53:Mena complex. Curr. Biol. *11*, 1645–1655.

Lee, C.C., Huang, C.C., Wu, M.Y., and Hsu, K.S. (2005). Insulin stimulates postsynaptic density-95 protein translation via the phosphoinositide 3-kinase-Akt-mammalian target of rapamycin signaling pathway. J. Biol. Chem. *280*, 18543–18550.

Man, H.Y., Lin, J.W., Ju, W.H., Ahmadian, G., Liu, L., Becker, L.E., Sheng, M., and Wang, Y.T. (2000). Regulation of AMPA receptor-mediated synaptic transmission by clathrin-dependent receptor internalization. Neuron *25*, 649–662.

Miki, H., Yamaguchi, H., Suetsugu, S., and Takenawa, T. (2000). IRSp53 is an essential intermediate between Rac and WAVE in the regulation of membrane ruffling. Nature *408*, 732–735.

Niell, C.M., Meyer, M.P., and Smith, S.J. (2004). In vivo imaging of synapse formation on a growing dendritic arbor. Nat. Neurosci. *7*, 254–260.

Nieuwkoop, P.D., and Faber, J. (1956). Normal Table of Xenopus laevis (Daudin) (Amsterdam: Elsevier-North Holland Publishing Co.).

Passafaro, M., Piech, V., and Sheng, M. (2001). Subunit-specific temporal and spatial patterns of AMPA receptor exocytosis in hippocampal neurons. Nat. Neurosci. *4*, 917–926.

Ruthazer, E.S., and Cline, H.T. (2002). Multiphoton imaging of neurons in living tissue: Acquisition and analysis of time-lapse morphological data. Real-Time Imaging *8*, 175–188.

Sanchez, A.L., Matthews, B.J., Meynard, M.M., Hu, B., Javed, S., and Cohen Cory, S. (2006). BDNF increases synapse density in dendrites of developing tectal neurons in vivo. Development *133*, 2477–2486.

Sin, W.C., Haas, K., Ruthazer, E.S., and Cline, H.T. (2002). Dendrite growth increased by visual activity requires NMDA receptor and Rho GTPases. Nature *419*, 475–480.

Skeberdis, V.A., Lan, J., Zheng, X., Zukin, R.S., and Bennett, M.V. (2001). Insulin promotes rapid delivery of N-methyl-D- aspartate receptors to the cell surface by exocytosis. Proc. Natl. Acad. Sci. USA *98*, 3561–3566.

Soltau, M., Richter, D., and Kreienkamp, H.J. (2002). The insulin receptor substrate IRSp53 links postsynaptic shank1 to the small G-protein cdc42. Mol. Cell. Neurosci. *21*, 575–583.

Song, J., Wu, L., Chen, Z., Kohanski, R.A., and Pick, L. (2003). Axons guided by insulin receptor in Drosophila visual system. Science *300*, 502–505.

Trachtenberg, J.T., Chen, B.E., Knott, G.W., Feng, G., Sanes, J.R., Welker, E., and Svoboda, K. (2002). Long-term in vivo imaging of experience-dependent synaptic plasticity in adult cortex. Nature *420*, 788–794.

Unger, J., McNeill, T.H., Moxley, R.T., 3rd, White, M., Moss, A., and Livingston, J.N. (1989). Distribution of insulin receptor-like immunoreactivity in the rat forebrain. Neuroscience *31*, 143–157.

Valenciano, A.I., Corrochano, S., de Pablo, F., de la Villa, P., and de la Rosa, E.J. (2006). Proinsulin/insulin is synthesized locally and prevents caspase- and cathepsin-mediated cell death in the embryonic mouse retina. J. Neurochem. *99*, 524–536.

Wan, Q., Xiong, Z.G., Man, H.Y., Ackerley, C.A., Braunton, J., Lu, W.Y., Becker, L.E., MacDonald, J.F., and Wang, Y.T. (1997). Recruitment of functional GABA(A) receptors to postsynaptic domains by insulin. Nature *388*, 686–690.

White, M.F. (2003). Insulin signaling in health and disease. Science *302*, 1710–1711.

Wu, G., Malinow, R., and Cline, H.T. (1996). Maturation of a central glutamatergic synapse. Science *274*, 972–976.

Zhang, L.I., Tao, H.W., and Poo, M. (2000). Visual input induces long-term potentiation of developing retinotectal synapses. Nat. Neurosci. *3*, 708–715.

Zhao, W., Chen, H., Xu, H., Moore, E., Meiri, N., Quon, M.J., and Alkon, D.L. (1999). Brain insulin receptors and spatial memory. Correlated changes in gene expression, tyrosine phosphorylation, and signaling molecules in the hippocampus of water maze trained rats. J. Biol. Chem. *274*, 34893–34902.